Hao, Z., Gao, Y., Ma, M., Green, S. M., Wang, J., Song, X., Dungait, J. A. J., Johnes, P. J., Xiong, B., Quine, T. A., Sun, X., Wen, X., & He, N. (2019). Using $\delta^{13}C$ to reveal the importance of different water transport pathways in two nested karst basins, Southwest China. *Journal of Hydrology*, *571*, 425-436. https://doi.org/10.1016/j.jhydrol.2019.01.070

Using $\delta^{13}C$ to reveal the importance of different water transport pathways in two nested karst basins, Southwest China

Zhuo Hao [1,2], Yang Gao [1,2*], Mingzhen Ma [1,2], Sophie M. Green[3], Jing Wang [1,2], Xianwei Song[1,2], Jennifer A. J. Dungait[3], Penny J. Johnes[4], Bailian Xiong[5], Timothy A. Quine[3], Xiaomin Sun [1,2*], Xuefa Wen [1,2], Nianpeng He[1,2]

[1] Key Laboratory of Ecosystem Network Observation and Modeling, Institute of Geographic Sciences and Natural Resources Research, CAS, Beijing 100101, P. R. of China; [2] College of Resources and Environment, University of Chinese Academy of Sciences, Beijing, 100190, P. R. of China; [3] Geography, CLES, Amory Building, University of Exeter, Rennes Drive, Exeter EX4 4RJ UK; [4] School of Geographical Sciences, University of Bristol, University Road, Bristol BS8 1SS, UK; [5] College of Resources and Environment, Zunyi Normal College, Zunyi, Guizhou, P. R of China

Abstract: This study used carbon (C) isotope sourcing to determine transport processes of dissolved inorganic carbon (DIC) from the land surface to river catchments in Southwest China. Both nested karst watersheds investigated (Chenqi and Houzhai) are representative of typical karst landform environments (e.g., primary

* Corresponding author

E-mail: gaoyang@igsnrr.ac.cn; sunxm@igsnrr.ac.cn

forest, secondary forest, and farmland). We measured DIC concentrations and the $\delta^{13}C$ values of rainfall, river water, groundwater, soil, and plants. To do so, we used IsoSource (a Visual Basic program) to determine source partitioning over time (seasonal) and across the two nested watersheds. In 2017, the mean DIC concentration was 0.06 ± 0.03 mmol L^{-1} and the rainfall $\delta^{13}C_{DIC}$ value was -14.4‰ ± 1.9‰. We found similar DIC concentrations in the surface and groundwater of both watersheds, ranging from 0.20 to 0.71 mmol L^{-1} (seasonal) and from -3.7‰ to -9.4‰ ($\delta^{13}C_{DIC}$) in the Chenqi catchment and from 0.33 to 0.60 mmol L^{-1} (seasonal) and from -10.3‰ to -6‰ ($\delta^{13}C_{DIC}$) in the Houzhai watershed. The average $\delta^{13}C$ values of soil and local plants were -24.6 ± 1.4‰ and -28.9 ± 1.2‰ in the Chenqi catchment and -25.8 ± 0.9‰ and -27.2 ± 1.8‰ in Houzhai watershed, respectively. In addition, carbonate bedrock and groundwater were the main sources of surface water in the Chenqi and Houzhai nested watersheds, both being greater than 30%. Source percentages were ~20% from atmospheric deposition and ~10% from soil. Furthermore, HCO_3^- was the predominant form of DIC (pH values > 8), and the contribution rates of dissolved carbonate minerals (HCO_3^-) were approximately 10.4% and 19.6% in the Chenqi catchment and the Houzhai watershed, respectively.

Keywords: carbon cycle; source partition; hydrological pathway; catchment

1. Introduction

Continual increases in atmospheric carbon dioxide (CO_2) that result in global warming and associated climate changes necessitate a deeper understanding of global

carbon (C) cycles (Huang et al., 2015; Zhao et al., 2015; Shin et al., 2011; Liu et al., 2010). Rivers play the leading role in transporting C from terrestrial to marine ecosystems in the global carbon cycle, being the main conduit of dissolved inorganic carbon (DIC) from the land surface to the oceans (McClanahan et al., 2016). Compared to organic and particulate fractions, DIC concentrations can provide more information on C sources and processes involved in riverine C cycles (Li et al., 2010; Cao et al., 2016; Brunet et al., 2009; Wachniew, 2006). The approximate global C flux from DIC through river transport is 0.4×10^{15} gC yr^{-1}, representing ~50% of the total C flux (Cole et al., 2007).

DIC concentrations are influenced by water-air CO_2 exchange processes, hydrologic inputs, vegetation, and carbonate weathering (McClanahan et al., 2016; Shin et al., 2011; Tobias and Böhlke, 2011; Brunet et al., 2009). Sources of DIC in river water include inputs from soil CO_2 (through groundwater), atmospheric CO_2 exchange, planktonic respiration, chemical weathering, and the dissolution of carbonate rocks. Recent studies have used stable isotopes to trace DIC sources which are usually characterized by $\delta^{13}C_{DIC}$ values. Each DIC source has a different $\delta^{13}C_{DIC}$ isotopic signature (from -26‰ to -9‰ for soil organic matter (SOM) (Wang et al., 2017a), -8‰ to -6‰ for atmospheric CO_2 and approximately 0‰ for carbonate rocks (Brunet et al., 2005). Moreover, C isotopes are used to assess riverine C transformation as well as follow the riverine DIC transport into oceans (Zeng et al, 2015 Brunet et al., 2005; Deirmendjian and Abril, 2018; Hu et al., 2017; Ye et al., 2017). Monitoring changes in spatial and temporal DIC concentrations and $\delta^{13}C_{DIC}$

values from inland water systems can provide a better understanding of C sources. At the same time, this approach is useful in revealing reaction pathways and transportation processes which would be difficult to discern with the normative carbonate systems involved in C cycling in freshwater systems (Cao et al., 2016; Tallini et al., 2014).

Approximately 67% of the global DIC in rivers is known to originate from soil CO_2 through C_3 plants, the typical photosynthetic pathway (van Geldern et al., 2015). C_3 plants have $\delta^{13}C$ values that range from -22‰ to -30‰, with an average approximate value of -27‰ (Marx et al., 2018; van Geldern et al., 2015). Along with photosynthesis, the main soil CO_2 transport pathways include rivers and streams. In stream zones, the contribution of groundwater to water flow is significant and the input of DIC-containing groundwater is derived from soil CO_2. Soil CO_2 tends to contain lower $\delta^{13}C_{DIC}$ values in river water because soil CO_2 mainly derives from the microbial degradation of SOM (Shin et al., 2011).

Karst zones are dynamic (McGee et al., 2010), being characterized by surface erosion and extensive subsurface drainage (Song et al., 2017; Chang et al., 2015). Moreover, karst aquifers are apt to form in areas of limestone and dolostone (Williams and Fong, 2010), wherein water is transported under conditions of dissolution. Water transport that takes place in bedrock, sinkholes, sinking streams, and runoff then percolates into groundwater and surface water (Lawhon. 2014). Such areas are environmentally sensitive and are known for their rapid hydrologic and chemical response to changing surface conditions (Yan et al., 2014; Li et al., 2012; Hartmann et

al., 2009; Macpherson et al., 2008). Karst landscapes comprise approximately 11.2% of the surface area of the planet, namely, approximately 15 million km^2 (Song et al., 2017; Dürr et al., 2005). Additionally, karst landscapes cover approximately 0.45 million km^2 in Southwest China (Yan et al., 2012). However, karst desertification (i.e., total soil loss) has increasingly become a serious problem in this region and could potentially become a global problem (e.g., changing climatic patterns) (Song et al., 2017).

Guizhou Province is suitable to study karst environments being located in the center of the South China Karst, the largest karst area in the world (Liao et al., 2015; Wang et al., 2017b; Zeng et al., 2015). Moreover, karst water resources account for 80% of the total water resources in this province (Li et al., 2018; Lu, 2007). This subtropical region has abundant rainfall (with an average of 1340 mm) as well as distinct rainy (May to August) and dry seasons. In addition, the surface-groundwater hydraulic system is a typical karst system, which facilitates the study of rainfall-driven hydrological C processes and will help in our understanding of C transport pathways and their implications. Accordingly, the objective of this study was to determine the importance of different transport pathways in surface and groundwater in a karst river basin (comprised of nested karst watersheds) using $\delta^{13}C_{DIC}$ to trace C sources. However, the present researches generally focused on relationship between surface water and groundwater or C sources of groundwater in karst watersheds (Zeng et al., 2015; Deirmendjian and Abril 2018; Marx et al. 2018). Therefore, the novelty of our research lies in using $\delta^{13}C_{DIC}$ from precipitation, plant,

soil to water throughout the whole watershed to trace the C transport and analyzing seasonal differences in C sources, thereby contributing to the further understanding of C transport and storage in large karst basins.

2. Materials and Methods

Study site

This study was conducted in the Houzhai watershed (80.65 km^2) (26°15′ N; 105°41′ E) located in Guizhou Province, Southwest China (Figure 1a). The bedrock type in the drainage area is predominantly limestone and dolomite of the Middle Triassic Guanling Formation (Liu et al., 2010a, 2010b; Zhao et al., 2010). The drainage basin ranges in altitude between 1218 and 1585 m above mean sea level (AMSL). This region is under the influence of a subtropical monsoon climate with an annual mean temperature of 15.2°C (Yan et al., 2012). Annual average precipitation is 1314.6 mm, and 85% of rainfall occurs during the rainy season (from May to October) (Yan et al., 2012). Tianlong Mountain (26°14′48″ N; 105°45′51″ E) is located within the Houzhai watershed. The area of this mountain is 0.5 km^2 and its altitude is 1460 m AMSL (Figure 1a). The mountain is covered by nearly 100% natural forests where the average tree height is 6.26 m, the average shrub layer is 1.3 m, and the average herbaceous layer is 0.4 m. In the study area, the black “residual” soil from 50 to 80 cm deep follows the Chinese soil taxonomic system. The Chenqi catchment (105°42' E; 26°14' N), which has an area of 1.31 km^2, is nested within the Houzhai watershed (see Figure 1b). Annual mean temperature is 14.2°C, mean precipitation is 1336 mm, and the altitude ranges from 1338 to 1491 m AMSL. The

land-use type of the Chenqi catchment is predominantly agricultural, including dry crops (i.e., maize; 56%), rice paddies (14%), abandoned areas dominated by shrubs (23%), and fruit trees (7%).

Water sampling

Surface and groundwater samples were collected from the Houzhai watershed and the Chenqi catchment twice a month from June 28th, 2016, to May 23rd, 2017. Figure 1b shows the 10 sampling locations in the Houzhai watershed: No. 1 is comprised of three sampling point (No. 1 surface water, No. 1G groundwater, and No. 1M the surface–groundwater mixed sampling points) and No. 2 to No. 10 are all comprised of surface water sampling points. Figure 1c shows that the Chenqi catchment is comprised of four groundwater sampling points (No. 1G, No. 3G, No. 6G, and No. 8G), six surface water sampling points (No. 1 through No. 6), and one surface-groundwater mixed sampling point (No. 7).

Samples were collected in 100 mL polyethylene plastic bottles and stored prior to analysis (4°C). Samples were filtered through a 0.45 μm membrane filter (Millipore) (Jiangsu Jiuding Group Co., Ltd., China). Water samples used to determine DIC, taken from the Millipore membranes, were thereafter heated to 80°C and maintained at this temperature for 8 h to remove impurities. We determined DIC using a Vario TOC Analyzer (Elementar, Langenselbold, Hesse, Germany) and $\delta^{13}C_{DIC}$ using a Finnigan MAT-252 mass spectrometer (Thermo Fisher Scientific, Darmstadt, Hesse, Germany) We measured K^+, Ca^{2+}, SiO_2, Na^+, and Mg^{2+} using an inductively coupled plasma optical emission spectrometer (ICP-OES) (Thermo Fisher Scientific,

Darmstadt, Hesse, Germany) and Cl^- and SO_4^{2-} using an ion chromatograph (Thermo Scientific Aquion IC, USA). We measured electrical conductivity (COND), redox potential (ORP), total dissolved solids (TDS), and water acidity (pH) using Ultrameter Ⅱ pH meters (Myron L company, Carlsbad, CA, USA). To collect rainfall samples, we installed a rain gauge on the roof of the station near No.1 sampling point in the test area of Houzhai watershed.

Plant and soil sampling

We collected plant and soil samples from the Chenqi catchment and the Tianlong Mountain in July 2016. For the Tianlong Mountain, we chose four height gradients (A, B, C, and D), and each height gradient was divided into four separate soil layers (0–10, 10–30, 30–50, and 50–100 cm) for soil sampling. Plant samples were collected from leaves, roots and twigs of different tree species. In the Chenqi catchment, two transects were established (Figure 1d) downslope on the hillside. Four quadrats were established on each transect from which plant and soil samples were collected. A total of 18 soil samples were collected from farmland, orchard, and forest land use types. Continuous soil cores were taken and subsampled at depth intervals of S1 (0–10 cm), S2 (10–30 cm), S3 (30–50 cm), and S4 (50–100 cm). Plant samples were collected as mixed samples according to type (i.e., tree, shrub, or herb). These plant samples were oven-dried at 60°C and then ground to <150 μm. Two milligrams of the subsamples were prepared for stable isotope analysis, and soil samples were then air-dried and ground to 150 μm. Finally, subsamples (3 g) were acidified (5% HCl) and then analyzed for $\delta^{13}C$ using the Finnigan MAT-252 mass spectrometer.

Statistical analysis

Isotopic mixing model

Utilizing one isotope system and three sources, we used the following mass balance equations to determine the proportions (f_A, f_B, and f_c) of isotopic signature sources (δ_A, δ_B, and δ_c), which coincide with the observed signatures of the mixture (δ_M):

$$\delta_M = f_A\delta_A + f_B\delta_B + f_C\delta_C$$

$$1 = f_A + f_B + f_C$$

however, with n (A, B, C, …) isotope systems and >n+1 sources, we were still able to apply the requirement for mass balance conservation to determine multiple combinations of source proportions that offer feasible solutions (Phillips and Gregg, 2003; Hao et al., 2018).

Stable isotope compositions of DIC in water, soil, and plant samples were expressed as conventional delta notations, the difference between measured ratios of the samples and references over the measured ratios of the references:

$$\delta^{13}C_{DIC}\,(‰) = \left(\frac{R_{Sample} - R_{Standard}}{R_{Standard}}\right) \times 1000$$

where R_{sample} and $R_{standard}$ represent $^{13}C/^{12}C$ in the samples and the standard references. Carbon isotope data were reported on the Vienna Pee Dee Belemnite (VPDB) (‰) scale, with a standard deviation (1σ) of 0.15‰ (Zhao et al., 2015).

Principal component analysis (PCA) and factor analysis were used with SPSS 17.0 software (SPSS Inc., Chicago, IL, the USA). The model outputs presented feasible ranges of isotope contributions given that the mass balance with qualitative statistics were calculated by IsoSource.

3 Results

3.1 Seasonal hydrochemical variations

Figure 2a shows the seasonal variation of pH ranges in the Houzhai watershed. The pH ranges were highest in autumn, namely, from 8.6 to 9.1 (except for the outliers) and lowest in summer, namely, from 8.3 to 8.5, and from 8.2 to 8.7 and from 8.2 to 8.5 in winter and spring, respectively. Figure 2b shows the seasonal variation of pH in the Chenqi catchment. Compared to the Houzhai watershed, pH ranges in the Chenqi catchment were narrow with the exception of spring. The highest values occurred in summer, namely, from 8.4 to 9.1 (except for the outliers) and the lowest in spring (from 7.8 to 8.2). Autumn and winter pH values were similar.

Figure 2c shows linear relationships between pH, COND, TDS, and ORP of 21 rainfall events, respectively. We found that COND and TDS values were positively correlated to pH values, while ORP values were negatively correlated to pH values. Table 1 shows the seasonal variation in water quality parameters of surface water, groundwater, and mixed sampling points in the Houzhai and Chenqi nested watersheds. As Table 1 shows, seasonal variation of ORP and pH in surface water, groundwater and mixed water were only slightly different in Houzhai watershed, while ORP values were much higher in summer and spring in Chenqi catchment. Furthermore, pH values in the Houzhai watershed were lower than Chenqi catchment with the exception of spring. Compared to other seasons, only COND and TDS values were higher in surface water than groundwater in the Houzhai watershed. Additionally, COND and TDS values in Chenqi were obviously

higher than the Houzhai watershed all year round. However, ORP values were particularly lower in the Chenqi catchment compared to the Houzhai watershed with the exception of spring in surface water.

3.2 Variations in dissolved inorganic carbon and $\delta^{13}C$

We collected data on 21 rainfall events from June 28th, 2016, to May 23rd, 2017, and found that DIC values for eight rain events were nearly 0 mmol L^{-1}. As Figure 3a shows, seasonal changes were significant, where the maximum concentration was 0.09 mmol L^{-1} in the spring of 2017 and the minimum concentration was nearly 0 mmol L^{-1} in the autumn of the same year. The average DIC concentration for all rain events was 0.02 ± 0.03 mmol L^{-1}. Additionally, DIC concentrations for rainfall events in 2017 were significantly higher compared to 2016, where the average DIC concentration for rain events from January to May 2017 was 0.06 ± 0.03 mmol L^{-1}. Figure 3b shows variation in $\delta^{13}C$ values for 11 rain events throughout 2016 to 2017. Seasonal variation was not obvious, wherein the maximum was -12.3‰ in the spring of 2017 and the minimum was -18.3‰ in the autumn of 2016. The average for all 11 rain events was -14.4‰ ± 1.9‰.

As Figure 4a shows, DIC concentrations in the Houzhai watershed ranged from 0.33 to 0.48 mmol L^{-1} during the summer, from 0.33 to 0.49 mmol L^{-1} during the autumn, from 0.39 to 0.58 mmol L^{-1} during the winter, and from 0.37 to 0.57 mmol L^{-1}during the spring. We found greater variation in DIC during the winter and spring compared to the summer and autumn. In sampling point No.1, surface water and groundwater exhibited similar variation, and DIC concentrations in groundwater were

241 higher than surface water.

242 Figure 4b shows DIC variation in the Chenqi catchment. We were able to obtain a
243 complete dataset of groundwater sampling points for all four seasons (winter, spring,
244 summer, and autumn). With the exception of No. 8G, namely, the groundwater
245 sampling points from the hilly area, all groundwater sampling points exhibited similar
246 variation, wherein the highest DIC concentration was measured in spring and lowest
247 in autumn. The No. 7 sampling point was also a surface and groundwater mixed
248 sampling point (where No. 6 and No. 6G were combined), and we found little
249 difference in DIC concentrations between surface and groundwater for all four
250 seasons. The maximum DIC concentration in the Chenqi catchment was 0.71 mmol
251 L^{-1}in spring and the minimum was 0.20 mmol L^{-1} in summer.

252 In both watersheds, DIC concentrations between surface water and groundwater
253 were only slightly different. Moreover, we found higher concentrations for both during
254 spring, when the averages were 0.50 and 0.56 mmol L^{-1}, and lower concentrations were
255 measured during autumn, when the averages were 0.39 and 0.41 mmol L^{-1} in the
256 Houzhai and Chenqi nested catchments, respectively. Surface water was abundant in
257 summer due to high rainfall frequency and abated in the autumn and winter, while
258 abundant groundwater was available all year around.

259 Figure 4c shows the 2016–2017 $\delta^{13}C$ values in the Houzhai watershed during the
260 autumn, winter, and spring. The range in variation of $\delta^{13}C$ values was from -10.3‰ to
261 -6‰, and the average $\delta^{13}C$ values in the autumn, winter, and spring were -9.0‰ ± 0.9‰,
262 -8.1‰ ± 1.0‰, and -7.4‰ ± 0.9‰, respectively. $\delta^{13}C$ values were more depleted in

autumn and were more enriched in spring, Figure 4d shows that $\delta^{13}C$ values in surface water and groundwater of the Chenqi catchment exhibited little difference, wherein the average $\delta^{13}C$ values were -7.4‰ ± 2.0‰ in surface water and -7.2‰ ± 2.2‰ in groundwater. Furthermore, different months yielded obviously different values in sampling point No. 6, where the maximum value was -3.7‰ in surface water in August and the minimum value was -9.4‰ in groundwater in August due to frequent rainfall.

3.3 Variation in $\delta^{13}C$ values for soil and vegetation

Figure 5a shows the $\delta^{13}C$ soil values of the four sampling depths of the different height gradients (from A to D) in the Tianlong Mountain, wherein the lowest values occurred in topsoil at all sampling points. The $\delta^{13}C$ values in sampling points B and C exhibited the same trend, namely, the deeper the soil layers were, the more depleted the $\delta^{13}C$ values were. The minimum value was -27.0‰ for the 0 to 10 cm soil layer in sampling point A, and the maximum value was -24.0‰ for the 50 to 100 cm soil layer in sampling point B. Figure 5b and 5c show the differences in two transects of a ditch between two hills in the Chenqi catchment. For example, the $\delta^{13}C$ value range in CQ-1 was from -28.3‰ to -22.6‰ and the $\delta^{13}C$ value range in CQ-2 was from -27.6 ‰ to -22.0‰. The averages of CQ-1 in S1 (0–10 cm), S2 (10–30 cm), S3 (30–50 cm), and S4 (50–100 cm) were -24.9‰, -24.8‰, -24.2‰, and -24.5‰, respectively, and the averages of CQ-2 were -25.5‰, -24.3‰, -24.7‰, and -24.6‰, respectively. We found that ^{13}C values were more enriched in the deeper soil layers (10–50 cm).

Figure 6a shows the $\delta^{13}C$ values of the four plant types in the Tianlong Mountain, which is near sampling point No. 8 in the Houzhai watershed. The highest $\delta^{13}C$ value was

285 -24.6‰ (cedar wood) and the lowest $\delta^{13}C$ value was -27.6‰ (*Broussonetia papyrifera*)
286 among the four plant types. Figure 6b shows the mixed samples of trees divided into
287 leaves, twigs, and roots, wherein the average $\delta^{13}C$ values were -30.2‰ ± 0.3‰, -28.7‰ ±
288 0.6‰, and -27.7‰ ± 0.5‰, respectively. Therefore, ^{13}C concentrations increased in the
289 roots of plants.
290
291 **4. Discussion**
292 **4.1 Inorganic river chemistry**
293 Dissolved and particulate C is likely associated with the chemical weathering of
294 basin soil and bedrock (McClanahan et al., 2016). COND is an indicator that reflects
295 ion changes under some conditions. Higher COND values indicate higher ionic
296 concentrations in water bodies, which may stem from the dissolution of carbonate
297 minerals. Both surface water and groundwater in the Chenqi catchment (TDS values:
298 510~723 $mg \cdot L^{-1}$) were much more carbonate-rich compared to the Houzhai watershed
299 (TDS values: 262~432 $mg \cdot L^{-1}$) all year around (Table 1). This indicated that there was
300 not only an increase in karst dissolution processes adding to the dissolved constituents
301 in the water, but other potential sources along the surface water path were
302 contributing COND and TDS values in karst water. These potential sources included
303 overland flow and anthropogenic impacts which also have influences on ionic
304 concentrations (COND) especially agricultural activities including potassium, nitrates,
305 and phosphates fertilizers (Lawhon, 2014; Moore et al., 2009).
306 The nature of redox reactions and redox-sensitive aqueous species is quite

different from most other reactions in aquifer systems (Liu et al., 2017). Therefore, it is necessary to set a unique redox status indicator in aquifer systems (Kumar and Riyazuddin, 2012). In water, ORP is strongly associated with temperature, pH, salinity, and dissolved oxygen concentrations (Liu et al., 2009; Li et al., 2014). The greater the dissolved oxygen (DO) is, the higher the ORP will be. As Table 1 shows, the Houzhai watershed yielded higher ORP compared to the Chenqi catchment; thus, its living conditions were better suited for aquatic organisms, when considering variations in pH and DO simultaneously.

In karst areas, such as the Houzhai and Chenqi nested watersheds, given the abundant carbonate bedrock, carbonates will help remove CO_2 from the system. Under most conditions, CO_2 is consumed because carbonate minerals dissolve in H_2O–CO_2 solutions, and pH will buffer to higher values due to adjustments in relevant reactions (chemical equilibrium).

As Figure 2c and Table 1 show, pH values were generally high in the sampling areas, and pH values in the Chenqi catchment were higher than in the Houzhai watershed. The CO_2 that escaped from streams in the Chenqi catchment reacted much more significantly than river water in the Houzhai watershed. Guizhou Province has a rich karst landscape, including carbonates and other minerals; therefore, water quality parameters, such as COND and TDS, are much higher in water than other areas. Moreover, these parameters have a direct effect on pH values in that they are higher than other areas (McClanahan et al., 2016; Lawhon, 2014; Mondal et al., 2010). However, previous literature reported that karst water bodies had been found to have

329 higher pH ranges in general (Hatcher, 2013).

330 **4.2 Using $\delta^{13}C$ values to distinguish between sources of dissolved inorganic**
331 **carbon**

332 Many internal and external factors, such as soil respiration, carbonate mineral
333 dissolution, atmospheric precipitation, and the pH value of water bodies, etc., have an
334 effect on $\delta^{13}C_{DIC}$ in water catchments (Shin et al., 2011; Doctor et al., 2008). In this
335 study, the average $\delta^{13}C$ values of surface water were lower than groundwater in the
336 Houzhai and Chenqi nested watersheds. This could be explained in that groundwater
337 may be derived more from "old" water in matrix pores that is more enriched in
338 $\delta^{13}C_{DIC}$ due to the longer time required for $CaCO_3$ dissolution to take place, while
339 river water has many sources, including groundwater inputs, atmospheric deposition,
340 soil water, and carbonate reactions. In order to determine $\delta^{13}C$ proportions from
341 various sources, the isotope model that we used to calculate results from IsoSource is
342 provided for the Houzhai and Chenqi nested watersheds (see Figure 7). As it pertains
343 to river water (surface water) and groundwater time spans, atmospheric deposition
344 results are typically taken from long-term monitoring, where, for example, average
345 soil $\delta^{13}C$ values are from -21‰ to -22‰ in karst areas of USA (McClanahan et al.,
346 2016). In China, the average soil $\delta^{13}C$ value is -24‰ (Zhao et al., 2015).

347 In this study, soil water was assumed to be -24‰ and carbonate mineral sources
348 were hypothesized to be 0‰ (Das et al., 2005; Hu et al., 2017; Li et al., 2010). The
349 main sources in the Chenqi catchment were groundwater and carbonate reactions,
350 wherein the mean percentages were 31.7% and 38.1%, respectively; the minimum

source was soil water, with a mean percentage of only 10.1% during the summer (Figure 7). In autumn, when stream flows were lower, percentages of groundwater were higher compared to carbonate reactions (Yan et al., 2014; Zhao et al., 2010). The proportion in the Houzhai watershed was similar to that of the Chenqi catchment, wherein the main sources were groundwater and carbonate reactions, which showed little differences between seasons. The mean proportions of the four sources were 32.4% in the autumn and 35.5% in the spring from groundwater, 20.5% in the autumn and 18.8% in the spring from atmospheric deposition, 11.4% in the autumn and 10.5% in the winter from soil water, and 35.7% in the autumn and 34.6% in the spring from carbonate reactions. In autumn, rainfall contributed more, which reduced the overall groundwater impact. Furthermore, winter and spring showed little seasonal differences in the difference in Houzhai watershed.

Figure7 shows the mean percentage of each source. All values are provided in Table 2, which also summarizes seasonal trends. To present model results more accurately, median values of model averages are provided along with the standard. The median value of carbonate reactions was highest (38% ± 13%) in summer and groundwater was highest (32% ± 24%) in autumn. The lowest DIC source was found in soil water, which likely derived from the interflow of water being infiltrated along slopes within the basin (9% ± 8%) in summer and (11% ± 9%) in the Chenqi catchment in autumn. In summer, rainfall was more frequent and subsequently surface water was more abundant; thus groundwater and soil water were lower than in the autumn. We found little differences between seasons in the Houzhai watershed. The

373 highest mean for all *in situ* carbonate reactions was 36%, and the lowest mean for all
374 soil was 8% as shown in Table 2.

375 **4.3 Influence and contribution rates of carbonate dissolution on dissolved**
376 **inorganic carbon concentrations**

377 River chemistry is strongly influenced by carbonate dissolution, which has an
378 obvious effect on pH value and supplies a large quantity of DIC in the form of
379 bicarbonates (Schulte et al., 2011). The study area lies within the carbonate area of the
380 region, and the distribution of pH in groundwater ranged from 7.9 to 9.0. Therefore,
381 the type of inorganic C in water is predominantly HCO_3^- (Doctor et al., 2007). COND
382 and pH values are shown in Table 1, which were completely consistent for both
383 sampling points. They showed that carbonate minerals control dissolution, including
384 the main DIC components in both the Chenqi catchment and the Houzhai watershed.

385 Cations (Ca^{2+}, Mg^{2+}, K^+, and Na^+) and anions (HCO_3^-, Cl^-, and SO_4^{2-}) were the
386 main ions found in the Chenqi catchment and the Houzhai watershed (Table 3). The
387 Piper diagram reflects not only the chemical composition of river water but also
388 distinguishes between different weathered sources of species composition (Stallard et
389 al., 1983). In the cationic ternary diagram (Figure 8), evaporite mineral weathering
390 products fall on the high Na^++K^+ line, while limestone weathering products fall on
391 Mg^{2+}-Ca^{2+} line. Due to dolomite characteristics, weathering products fall in the
392 middle of the Mg^{2+} and Ca^{2+} (Ca: Mg = 1:1) lines(Li et al., 2010).

393 Furthermore, the weathering products of silicate minerals fall on the Mg^{2+}-Ca^{2+}
394 line, which is relatively biased towards one side of Na^++K^+. In the anion ternary graph,

the weathering material of pure carbonates is primarily HCO_3^-; thus, the data points fall at the relatively high end of HCO_3^-. The weathering products of evaporated salt minerals fall on the Cl^-+ SO_4^{2-} line, and the proportion is relatively high, while the weathering of silicate minerals causes both HCO_3^- and SiO_2 to be present in river systems. In this study, the proportion of Ca^{2+} and Mg^{2+} were higher than Na^++K^+. In particular, Ca^{2+}, HCO_3^-, and SO_4^{2-} were obviously higher than Cl^- and Mg^{2+} in the Chenqi catchment and the Houzhai watershed, which suggested that river water in these two nested watersheds are controlled by carbonates, silicate minerals, and small amounts of evaporites.

In order to further quantify the influence of different rock types on the main ions found in rivers, we used the main ion concentrations (Ca^{2+}, Mg^{2+}, K^+, Na^{2+}, Cl^-, SiO_2, and HCO_3^-) of surface water in the Chenqi catchment and the Houzhai watershed for PCA and factor analysis of river water chemistry as shows in Table3 and Figure 9. In the Chenqi catchment, as Figure 9 shows, the cumulative contribution rate of the first three variables reached 79.6% (<80%), but eigenvalues from the extraction factor were less than 1 of the fourth variable, and therefore deleted. Factor 1 was highly correlated to Ca^{2+}, Mg^{2+}, Na^{2+}, and SiO_2, indicating that the dissolution of silicate minerals contributes to chemical weathering in the sampling areas. Factor 2 was more significantly correlated to K^+ and HCO_3^-, and Factor 3 was more significantly correlated to Cl^- and SO_4^{2-}, indicating that the contribution of dissolved carbonate minerals was relatively high compared to silicate minerals (Figure 9). Bare carbonate rocks accounted for almost 75% of the study area, which suggested that carbonate

417 dissolution should play a key role in rock weathering (Cao et al., 2005; Li et al., 2010).
418 In the Houzhai watershed, as Figure 9 shows, the cumulative contribution rate of the
419 first three variables reached 81.2% (>80%), and the relationship between each factor
420 was similar to the Chenqi catchment. The squares of each variable factor load divided
421 by the common variance is the relative variance contribution of dissolution of each
422 type of rock to each variable. After calculations, the contribution rates of dissolved
423 carbonate minerals to HCO_3^- were approximately 10.4% and 19.6% in the Chenqi
424 catchment and the Houzhai watershed, respectively.

425 **4.4 $\delta^{13}C$ characteristics of vegetation and soil**

426 The $\delta^{13}C$ values of the C_3 and C_4 photosynthetic pathway plants were distinctly
427 different, namely, the average value of C_3 plants is -27.1‰ (from -21‰ to -35‰) and
428 the average value of C_4 plants is -13.1‰ (from -10‰ to -14‰) (Rouw et al., 2015). In
429 our study, all plant $\delta^{13}C$ values in the Houzhai watershed were from -24.6‰ to -27.6‰
430 and all plant $\delta^{13}C$ values in the Chenqi catchment were from -27.7‰ to -30.2‰. For
431 CQ-1, soil $\delta^{13}C$ values were more enriched in the deeper soil layers, with an order
432 rank of S1<S2<S4<S3, and the order rank of soil $\delta^{13}C$ values in CQ-2 was S1<
433 S3<S4<S2. The reason for this could potentially be that surface soil is easily
434 transported by rain, promoting nutrient accumulation in deeper soil layers (10–50 cm)
435 in karst areas. The 0–10 cm soil layer in these soil profiles had the lowest $\delta^{13}C$ values
436 of the corresponding profile. This is due to the fact that the top of the soil profile had
437 a relatively large amount of undecomposed plant residue and better preserved plant
438 $\delta^{13}C$ signatures, while underneath the surface soil, due to the uneven distribution of

plant roots, different degrees of plant residue decomposition and differences in organic or acid species in the soil itself, etc., could lead to differences in $\delta^{13}C$ soil sample values (Wynn et al., 2006; Wang et al., 2008).

The average $\delta^{13}C$ value of SOC for the four soil profiles was -24.6‰±1.4‰ in the Chenqi catchment, with an $\delta^{13}C$ enrichment value of 4‰ compared to the weighted average $\delta^{13}C$ value of local plants (-28.9‰±1.2‰). This trend was also seen in the Houzhai watershed, with an average value of -25.8‰±0.9‰, an increase of nearly 2‰ compared to local plants. During isotope fractionation, which occurs through microbial decomposition of organic matter and leads to the uneven distribution of ^{13}C and ^{12}C during the different C phases between reactants and products, there is relatively more ^{12}C in released CO_2, whereas ^{13}C is more prevalent in C derived from microbial biomass, eventually being returned as SOM (Luo and Wang, 2009; Li et al., 2012). Furthermore, even for individual plants, ^{13}C tends to concentrate in root systems followed by twigs and leaves, and this is because the lighter ^{12}C isotope exits plants through transpiration. In order to fully understand C cycling, more research is required on interannual changes, photosynthesis and transpiration of C_3 and C_4 plants, and soil microbial respiration to better understand internal C cycling dynamics that could influence DIC sources, transportation, and storage, which could even lead to an improvement in global C sink estimations (Figure 10).

5. Conclusions

Carbonate karst environments may play an indispensable role in the global C

budget. Investigations into the impacts of karst watersheds such as C transportation and storage within this system on a local level are vital to understanding the global C cycle. International and domestic academics have provided credible scientific data regarding many aspects of karst watersheds in China. However, additional research is needed for a better comprehensive understanding of DIC and its sources in this type of system. In this study, carbonate reactions and groundwater were the main sources of river water in Houzhai and Chenqi watersheds, whose proportions were both greater than 30% in river water. Sources proportions were influenced by seasonality which related to the frequency of rainfall, especially regarding groundwater and soil water. Furthermore, DIC mainly exists in the form of HCO_3^- in the sampling areas of this study, of which the contribution rate of dissolved carbonate minerals (HCO_3^-) was approximately 10.4%-19.6%. Silicate minerals and evaporites had a negligible effect on DIC in the nested watersheds investigated in this study. The amount of carbonate mineral dissolution had a significant influence on surface water and groundwater (in the form of a C sink) under karst hydrological conditions. Additionally, water-soil and soil-plant processes together comprised the complete karst eco-hydrological C cycle in this study which is not mentioned in other studies at present. More relevant studies, however, are required in order to gain a more comprehensive understanding of biogeochemical cycles in large karst-influenced watersheds.

Acknowledgments

The authors of this study would like to thank all anonymous reviewers for their helpful remark and Puding Karst Ecosystem Research Station, Chinese Ecosystem

Research Network, Chinese Academy of Sciences. This study was financially supported by the National Nature Science Foundation of China (No.41571130043, 41871080 and 31570465) and the Youth Innovation Promotion Association of the Chinese Academy of Sciences.

References

Brunet, F., Gaiero, D., Probst, J. L., Depetris, P.J., Lafaye, F. G., Stille, P., 2005. delta C-13 tracing of dissolved inorganic carbon sources in Patagonian rivers (Argentina). Hydrol Process 19, 3321-3344. https://doi.org/10.1002/hyp.5973.

Brunet, F., Dubois, K., Veizer, J., Ndondo, G. R. N., Ngoupayou, J. R. N., Boeglin, J. L., Probst, J. L. 2009. Terrestrial and fluvial carbon fluxes in a tropical watershed: nyong basin, cameroon. Chemical Geology, 265(3), 563-572. https://doi.10.1016/j.chemgeo.2009.05.020.

Cao, X. X., Wu, P., Han, Z. W., Tu, H., Zhang, S. 2016. Factors controlling the isotope composition of dissolved inorganic carbon in a karst-dominated wetland catchment, Guizhou Province, Southwest China, Environmental Earth Sciences, 75(14), https://doi.Artn 110310.1007/S12665-016-5899-4.

Cole, J. J., Prairie, Y. T., Caraco, N. F., McDowell, W. H., Tranvik, L. J., Striegl, R. G., Duarte, C. M., Kortelainen, P., Downing, J. A., Middelburg, J. J., Melack, J., 2007. Plumbing the global carbon cycle: Integrating inland waters into the terrestrial carbon budget, Ecosystems, 10(1), 171-184. https://doi.10.1007/s10021-006-9013-8.

Chang, Y., Wu, J. C., Jiang, G. H. 2015. Modeling the hydrological behavior of a karst

505 spring using a nonlinear reservoir-pipe model, Hydrogeology Journal, 23(5),
506 1-14. https://doi. 10.1007/s10040-015-1241-6.
507 Das, A., Krishnaswami, S., Bhattacharya, S. K., 2005. Carbon isotope ratio of
508 dissolved inorganic carbon (DIC) in rivers draining the Deccan Traps, India:
509 Sources of DIC and their magnitudes. Earth Planet Sc Lett 236, 419-429.
510 https://doi. 10.1016/j.epsl.2005.05.009.
511 Deirmendjian, L., Abril, G., 2018. Carbon dioxide degassing at the
512 groundwater-stream-atmosphere interface: isotopic equilibration and
513 hydrological mass balance in a sandy watershed. J Hydrol 558, 129-143.
514 https://doi. 10.1016/j.jhydrol.2018.01.003.
515 Doctor, D. H., Kendall, C., Sebestyen, S. D., Shanley, J. B., Ohte, N., & Boyer, E. W.
516 2010. Carbon isotope fractionation of dissolved inorganic carbon (dic) due to
517 outgassing of carbon dioxide from a headwater stream. Hydrological Processes,
518 22(14), 2410-2423. https://doi. 10.1002/hyp.6833.
519 Dürr, H. H., Meybeck, M., Dürr, S. H. 2005. Lithologic composition of the earth's
520 continental surfaces derived from a new digital map emphasizing riverine
521 material transfer. Global Biogeochemical Cycles. 19(4).
522 https://doi.10,1029/2005GB002515.
523 Gao, Y., He, N. P., Wang, Q. F., Miao, C. Y. 2013. Increase of External Nutrient Input
524 Impact on Carbon Sinks in Chinese Coastal Seas. Environmental Science &
525 Technology, 47(23), 13215-13216. https://doi. 10.1021/es4045743.
526 Gao, Y., Yu, G. R., Yang, T. T., Jia, Y. L., He, N. P., Zhuang, J. 2016. New insight into

527 global blue carbon estimation under human activity in land-sea interaction area:
528 A case study of China. Earth-Science Reviews, 159, 36-46. https://doi.
529 10.1016/j.earscirev.2016.05.003.
530 Hao, Z., Gao, Y., Sun, X. M., Wen, X. F. 2018. Differential isotopic characteristics of
531 eco-hydrologic processes in a subtropical watershed, China. Ecohydrology,
532 11(4). https://doi. Unsp E194410.1002/Eco.1944.
533 Hartmann, J., Jansen, N., Durr, H. H., Kempe, S., Kohler, P. 2009. Global
534 CO2-consumption by chemical weathering: What is the contribution of highly
535 active weathering regions? Global and Planetary Change, 69(4), 185-194.
536 https://doi.10.1016/j.gloplacha.2009.07.007.
537 Hatcher, B. E., 2013. Sources of CO2 Controlling the Carbonate Chemistry of the
538 Logsdon River, Mammoth Cave, Kentucky. M.S. Thesis, Department of
539 Geography and Geology, Western Kentucky University, Bowling Green, KY.
540 Hu, Y., Lu, Y.H., Liu, C.K., Shang, P., Liu, J., Zheng, C.M. 2017. Sources and
541 Dynamics of Dissolved Inorganic Carbon, Nitrogen, and Phosphorus in a
542 Large Agricultural River Basin in Arid Northwestern China. Water, 9(6).
543 https://doi. Artn 415.
544 Huang, F., Zhang, C. L., Xie, Y. C., Li, L., Cao, J. H. 2015. Inorganic carbon flux and
545 its source in the karst catchment of Maocun, Guilin, China. Environmental
546 Earth Sciences, 74(2), 1079-1089. https://doi.10.1007/s12665-015-4478-4.
547 Huang, Q. B., Qin, X. Q., Yang, Q. Y., Liu, P. Y., Zhang, J. S. 2016. Identification of
548 dissolved sulfate sources and the role of sulfuric acid in carbonate weathering

549 using delta C-13(DIC) and delta S-34 in karst area, northern China,
550 Environmental Earth Sciences, 75(1). https://doi. ARTN 51
551 10.1007/s12665-015-4869-6.
552 Kumar, A. R., Riyazuddin, P. 2012. Seasonal variation of redox species and redox
553 potentials in shallow groundwater: A comparison of measured and calculated
554 redox potentials. Journal of Hydrology, 444, 187-198. https://doi.
555 10.1016/j.jhydrol.2012.04.018.
556 Lawhon N. 2014. Investigating Telogenetic Karst Aquifer Processes and Evolution in
557 South-central Kentucky, U.S., Using High-resolution Storm Hydrology and
558 Geochemical Monitoring, MS in Geoscience, Department of Geography and
559 Geology, Western Kentucky University.
560 http://digitalcommons.wku.edu/theses/1324
561 Li, S. L., Liu, C. Q., Li, J., Lang, Y. C., Ding, H., Li, L. B. 2010. Geochemistry of
562 dissolved inorganic carbon and carbonate weathering in a small typical karstic
563 catchment of Southwest China: Isotopic and chemical constraints, Chemical
564 Geology, 277(3-4), 301-309, https://doi.10.1016/j.chemgeo.2010.08.013.
565 Li, T. Y., Li, H. C., Xiang, X. J., Kuo, T. S., Li, J. Y., Zhou, F. L., Chen, H. L., Peng, L.
566 L. 2012. Transportation characteristics of delta C-13 in the
567 plants-soil-bedrock-cave system in Chongqing karst area, Science China Earth
568 Sciences, 55(4), 685-694, https://doi.10.1007/s11430-011-4294-y.
569 Li, X., Blancheton, J. P., Liu, Y., Triplet, S., Michaud, L. 2014. Effect of
570 oxidation-reduction potential on performance of European sea bass

(Dicentrarchus labrax) in recirculating aquaculture systems. Aquaculture International, 22(4), 1263-1282. https://doi.10.1007/s10499-013-9745-3.

Li, X. X., Wu, P., Han, Z. W., Zha, X. F., Ye, H. J., Qin, Y. J. 2018. Effects of mining activities on evolution of water quality of karst waters in Midwestern Guizhou, China: evidences from hydrochemistry and isotopic composition. Environmental Science and Pollution Research, 25(2), 1220-1230. https://doi.10.1007/s11356-017-0488-y.

Liao, H. K., Long, J., Li, J. 2015. Soil organic carbon associated in size-fractions as affected by different land uses in karst region of Guizhou, Southwest China. Environmental Earth Sciences, 74(9), 6877-6886. https://doi.10.1007/s12665-015-4690-2

Liu, L. H., Shu, L. C., Chen, X. H., Oromo, T. 2010. The hydrologic function and behavior of the Houzhai underground river basin, Guizhou Province, southwestern China. Hydrogeology Journal, 18(2), 509-518. https://doi.10.1007/s10040-009-0518-z.

Liu, X. Q., Wang, J., Zhang, D., Li, Y. T. 2009. Grey relational analysis on the relation between marine environmental factors and oxidation-reduction potential. Chinese Journal of Oceanology and Limnology, 27(3), 583-586. https://doi.10.1007/s00343-009-9152-9

Liu, X. X., Yuan, S. H., Tong, M., Liu, D., 2017. Oxidation of trichloroethylene by the hydroxyl radicals produced from oxygenation of reduced nontronite. Water Research, 113, 72-79. https://doi. 10.1016/j.watres.2017.02.012

593 Liu, Z. H., Dreybrodt, W., Wang, H. J. 2010. A new direction in effective accounting
594 for the atmospheric CO2 budget: Considering the combined action of
595 carbonate dissolution, the global water cycle and photosynthetic uptake of DIC
596 by aquatic organisms. Earth-Science Reviews, 99(3-4), 162-172. https://doi.
597 10.1016/j.earscirev.2010.03.001
598 Lu, Y. R., 2007. Karst water resources and geo-ecology in typical regions of China.
599 Environmental Geology, 51(5), 695-699. https://doi.
600 10.1007/s00254-006-0381-3.
601 Luo, W. J., Wang, S. J. 2009. Transmission of delta C-13 signals and its paleoclimatic
602 implications in Liangfeng Cave system of Guizhou Province, SW China.
603 Environmental Earth Sciences, 59(3), 655-661. https://doi.
604 10.1007/s12665-009-0062-0.
605 Macpherson, G. L., Roberts, J. A., Blair, J. M., Townsend, M. A., Fowle, D. A.,
606 Beisner, K. R. 2008. Increasing shallow groundwater CO2 and limestone
607 weathering, Konza Prairie, USA. Geochimica Et Cosmochimica Acta, 72(23),
608 5581-5599. https://doi. 10.1016/j.gca.2008.09.004
609 Marx, A., Conrad, M., Aizinger, V., Prechtel, A., van Geldern, R., Barth, J. A. C. 2018.
610 Groundwater data improve modelling of headwater stream CO2 outgassing
611 with a stable DIC isotope approach. Biogeosciences 15, 3093-3106. https://doi.
612 10.5194/bg-15-3093-2018.
613 McClanahan, K., Polk, J., Groves, C., Osterhoudt, L., Grubbs., S. 2016. Dissolved
614 inorganic carbon sourcing using C-13(DIC) from a karst influenced river

615 system, Earth Surface Processes and Landforms, 41(3), 392-405.
616 https://doi.10.1002/esp.3856.
617 McGee, D. K., Wynn, J. G., Onac, B. P., Harries, P. J., Rothfus, E. A. 2010. Tracing
618 groundwater geochemistry using delta C-13 on San Salvador Island
619 (southeastern Bahamas): implications for carbonate island hydrogeology and
620 dissolution, Carbonates and Evaporites, 25(2), 91-105.
621 https://doi.10.1007/s13146-010-0013-6.
622 Mondal, N. C., Singh, V. P., Singh, V. S., Saxena, V. K. 2010. Determining the
623 interaction between groundwater and saline water through groundwater major
624 ions chemistry. Journal of Hydrology, 388(1-2), 100-111.
625 https://doi.10.1016/j.jhydrol.2010.04.032
626 Phillips, D. L., Gregg, J. W. 2003. Source partitioning using stable isotopes: coping
627 with too many sources, Oecologia, 136(2), 261-269.
628 https://doi.10.1007/s00442-003-1218-3.
629 Rouw, A., Soulileuth, D., Huon, B. S. 2015. Stable carbon isotope ratios in soil and
630 vegetation shift with cultivation practices (Northern Laos), Agriculture
631 Ecosystems & Environment, 200, 161-168. https://doi.
632 10.1016/j.agee.2014.11.017
633 Schulte, P., van Geldern, R., Freitag, H., Karim, A., Negrel, P., Petelet-Giraud, E.,
634 Barth, J. A. C. 2011. Applications of stable water and carbon isotopes in
635 watershed research: Weathering, carbon cycling, and water balances.
636 Earth-Science Reviews, 109(1-2), 20-31.

637 https://doi.10.1016/j.earscirev.2011.07.003.
638 Shin, W. J., Chung, G. S., Lee, D., & Lee, K. S. 2011. Dissolved inorganic carbon
639 export from carbonate and silicate catchments estimated from carbonate
640 chemistry and δ13CDIC, Hydrology & Earth System Sciences, 15(8),
641 2551-2560. https://doi.10.5194/hessd-8-1799-2011.
642 Song, X. W., Gao, Y., Wen, X. F., Guo, D. L., Yu, G. R., He, N. P., Zhang, J. Z. 2017.
643 Carbon sequestration potential and its eco-service function in the karst area,
644 China. Journal of Geographical Sciences, 27(8), 967-980.
645 https://doi.10.1007/s11442-017-1415-3.
646 Stallard, R. F., Edmond, J. M. 1983. Geochemistry of the Amazon .2. The Influence of
647 Geology and Weathering Environment on the Dissolved-Load. Journal of
648 Geophysical Research-Oceans, 88(Nc14), 9671-9688.
649 https://doi.10.1029/Jc088ic14p09671.
650 Tallini, M., Falcone, R. A., Carucci, V., Falgiani, A., Parisse, B., Petitta, M. 2014.
651 Isotope hydrology and geochemical modeling: new insights into the recharge
652 processes and water-rock interactions of a fissured carbonate aquifer (Gran
653 Sasso, central Italy), Environmental Earth Sciences, 72(12), 4957-4971,
654 https://doi.10.1007/s12665-014-3364-9.
655 Tobias, C., Bohlke, J. K. 2011. Biological and geochemical controls on diel dissolved
656 inorganic carbon cycling in a low-order agricultural stream: Implications for
657 reach scales and beyond. Chemical Geology, 283(1-2), 18-30.
658 https://doi.10.1016/j.chemgeo.2010.12.012.

van Geldern, R., Schulte, P., Mader, M., Baier, A., Barth, J. A. C. 2015. Spatial and temporal variations of pCO(2), dissolved inorganic carbon and stable isotopes along a temperate karstic watercourse, Hydrological Processes, 29(15), 3423-3440. https://doi.10.1002/hyp.10457.

Wang, G., Feng, X., Han, J., Zhou, L., Tan, W., Su, F. 2008. Paleovegetation reconstruction using delta C-13 of Soil Organic Matter. Biogeosciences, 5(5), 1325-1337. https://doi. 10.5194/bg-5-1325-2008.

Wang, Y. F., Chen, L. D., Gao, Y., Chen, S. B., Chen, W. L., Hao, Z., Jia, J .J., Han, N., 2017a. Geochemical isotopic composition in the Loess Plateau and corresponding source analyses: A case study of China's Yangjuangou catchment. Science of the Total Environment, 581, 794-800. https://doi.10.1016/j.scitotenv.2017.01.012.

Wang, Z. M., Rawal, K., Hu, L. B., Yang, R. D., Yang, G. L., 2017b. A study of dissolution and water-bearing characteristics of the restricted platform dolomite facies in the karst areas of Guizhou, China. Environmental Earth Sciences, 76(3). https://doi. Artn 12410.1007/S12665-017-6419-X.

Williams P. W., Fong, Y. T., 2010. Karst Regions of the World. Circle of Blue online at:http://www.circleofblue.org/waternews/wp-content/uploads/2010/01/world-karst-map-web-1.12.jpg, (Accessed March 29, 2013).

Wynn, J. G., Harden, J. W., Fries, T. L. 2006. Stable carbon isotope depth profiles and soil organic carbon dynamics in the lower Mississippi Basin. Geoderma, 131(1-2), 89-109. https://doi.10.1016/j.geoderma.2005.03.005.

681 Yan, J. H., Li, J. M., Ye, Q., Li, K. 2012. Concentrations and exports of solutes from
682 surface runoff in Houzhai Karst Basin, southwest China, Chemical Geology,
683 304, 1-9. https://doi.10.1016/j.chemgeo.2012.02.003.
684 Yan, J. H., Wang, W. T., Zhou, C. Y., Li, K., Wang, S. J. 2014. Responses of water
685 yield and dissolved inorganic carbon export to forest recovery in the Houzhai
686 karst basin, southwest China, Hydrological Processes, 28(4), 2082-2090.
687 https://doi.10.1002/hyp.9761.
688 Ye, F., Guo, W., Shi, Z., Jia, G. D., Wei, G. J., 2017. Seasonal dynamics of particulate
689 organic matter and its response to flooding in the Pearl River Estuary, China,
690 revealed by stable isotope (delta C-13 and delta N-15) analyses. J Geophys
691 Res-Oceans 122, 6835-6856. https://doi. 10.1002/2017JC012931.
692 Zeng, C., Liu, Z. H., Yang, J. W., Yang, R. 2015. A groundwater conceptual model and
693 karst-related carbon sink for a glacierized alpine karst aquifer, Southwestern
694 China, Journal of Hydrology, 529, 120-133.
695 https://doi.10.1016/j.jhydrol.2015.07.027.
696 Zhao, M., Liu, Z. H., Li, H. C., Zeng, C., Yang, R., Chen, B., Yan, H. 2015. Response
697 of dissolved inorganic carbon (DIC) and delta C-13(DIC) to changes in
698 climate and land cover in SW China karst catchments. Geochimica Et
699 Cosmochimica Acta, 165, 123-136. https://doi. 10.1016/j.gca.2015.05.041.
700 Zhao, M., Zeng, C., Liu, Z. H., Wang S. J. 2010. Effect of different land use/land
701 cover on karst hydrogeochemistry: A paired catchment study of Chenqi and
702 Dengzhanhe, Puding, Guizhou, SW China, Journal of Hydrology, 388(1-2),

121-130. https://doi.10.1016/j.jhydrol.2010.04.034.

Table 1 Water quality parameters of surface water, groundwater and mixed water in Houzhai and Chenqi.

Sample	Summer				Autumn			
Point	COND (uS cm^{-1})	TDS ($mg.L^{-1}$)	ORP (mv)	PH	COND (uS cm^{-1})	TDS ($mg.L^{-1}$)	ORP (mv)	PH
HZ-S	410	276	216	7.9	391	262	187	8.6
HZ-G	397	266	219	7.9	423	285	186	8.8
HZ-M	403	271	216	8.3	456	308	181	8.8
CQ-S	452	510	213	9.0	836	581	124	8.9
CQ-G	491	586	194	9.0	780	542	130	9.0
CQ-M	747	514	203	9.0	1042	723	134	8.9
Sample	Winter				Spring			
Point	COND (uS cm^{-1})	TDS ($mg.L^{-1}$)	ORP (mv)	PH	COND (uS cm^{-1})	TDS ($mg.L^{-1}$)	ORP (mv)	PH
HZ-S	396	266	211	8.4	467	315	208	8.3
HZ-G	451	304	212	8.5	635	432	219	8.2
HZ-M	405	272	211	8.5	626	426	223	8.3
CQ-S	770	526	125	8.9	838	573	218	7.9
CQ-G	740	514	127	9.1	855	596	217	8.1
CQ-M	787	557	122	9.1	896	615	217	8.2

(Note: pH, COND, TDS and ORP were measured by Ultrameter Ⅱ (Myron L company USA. HZ-S values represent the average for all the surface water points (No. 1 through No. 10) in the Houzhai watershed; HZ-G values represent the average for No.1G in different months; HZ-M values represent the average for No.1M in different months. CQ-G values represent the average of the four groundwater sampling points in different months; CQ-S values represent the average of the six surface water sampling points in different months and CQ-M values represent the average for the No.7 in different months.)

715

716

717 **Table 2 Seasonal trends of model results for Chenqi and Houzhai**

718

		Ground water		Atmosphere deposition		Soil water		Carbonate reaction	
		value	median standard	value	median standard	value	median standard	value	median standard
(Chenqi)	Median	28%	23%	18%	15%	9%	8%	38%	13%
Summer	Minimum	0%		0%		0%		6%	
	Maximum	94%		60%		31%		69%	
	Median	32%	24%	20%	16%	11%	9%	29%	14%
Fall	Minimum	0%		0%		0%		0%	
	Maximum	93%		64%		37%		61%	
(Houzhai)	Median	29%	23%	18%	15%	10%	8%	36%	13%
Fall	Minimum	0%		0%		0%		4%	
	Maximum	95%		61%		34%		65%	
	Median	30%	25%	17%	14%	9%	8%	36%	15%
Winter	Minimum	0%		0%		0%		0%	
	Maximum	97%		57%		30%		67%	
	Median	32%	24%	17%	13%	10%	8%	36%	16%
Spring	Minimum	0%		0%		0%		0%	
	Maximum	92%		53%		31%		66%	

719 (Note: IsoSource calculation automatic generated results. Groundwater, atmosphere deposition, soil water and carbonate
720 reactions as the four sources of river water in this study. The median, minimum and maximum of possibility within
721 the river routinely produced and median standard contributions of 20–25% and 8–16%, respectively).

722

723

724

725

726

727

728

Table 3 Cations and anions concentrations of surface water, groundwater in Houzhai and Chenqi.

Points	Summer				Autumn			
Concentrations (mmol • L^{-1})	CQ-S	CQ-G	HZ-S	HZ-G	CQ-S	CQ-G	HZ-S	HZ-G
Ca^{2+}	4.55	2.86	1.06	1.28	6.73	2.89	1.74	1.01
Mg^{2+}	2.17	1.13	0.83	0.91	3.38	1.33	0.96	0.87
Na^{+}	0.29	0.08	0.13	0.15	0.32	0.09	0.19	0.16
K^{+}	0.38	0.06	0.07	0.07	0.13	0.05	0.11	0.08
SO_4^{2-}	1.36	2.97	0.60	0.60	2.68	1.31	0.90	0.60
Cl^{-}	0.15	0.19	0.19	0.30	0.18	0.22	0.25	0.21
HCO_3^{-}	0.45	0.45	0.51	0.57	0.39	0.41	0.54	0.50
SiO_2	0.19	0.14	0.02	0.05	0.28	0.14	0.09	0.07
season	Winter				Spring			
Point	CQ-S	CQ-G	HZ-S	HZ-G	CQ-S	CQ-G	HZ-S	HZ-G
Ca^{2+}	2.44	2.64	1.19	1.00	3.41	3.34	2.25	1.98
Mg^{2+}	1.16	1.38	0.78	0.86	1.30	1.74	1.23	1.19
Na^{+}	0.07	0.09	0.21	0.20	0.15	0.59	0.37	0.54
K^{+}	0.03	0.03	0.10	0.05	0.16	0.06	0.15	0.07
SO_4^{2-}	1.97	2.61	1.19	0.77	3.10	2.44	1.61	0.99
Cl^{-}	0.17	0.11	0.31	0.31	0.23	0.13	0.39	0.39
HCO_3^{-}	0.39	0.44	0.52	0.57	0.55	0.55	0.56	0.58
SiO_2	0.13	0.14	0.06	0.06	0.17	0.15	0.05	0.06

(Note: HZ-S values represent the average for all the surface water points (No. 1 through No. 10) in the Houzhai watershed; HZ-G values represent the average for No.1G in different months. CQ-G values represent the average of the four groundwater sampling points in different months; CQ-S values represent the average of the six surface water sampling points in different months.)

Figure Caption

Figure 1 (a) Study sites location in Puding County, Guizhou. (b) The water sampling points in Houzhai watershed. (c) The water sampling points in Chenqi catchment. (d) The soil sampling points in Chenqi catchment.

Figure 2 (a) The seasonal variation of pH values in Houzhai. (b) The seasonal variation of pH values in Chenqi.(c) Correlation between pH with water quality parameters of atmospheric deposition from 2016 to 2017.

Figure 3(a) Variation of [DIC] of rainfall during 2016 to 2017. (b) The variation of $\delta^{13}C_{DIC}$ of rainfall during 2016 to 2017.

Figure 4 (a) The seasonal variation of DIC in Houzhai watershed. (b) The seasonal variation of DIC in Chenqi catchment. (c) Seasonal variation of $\delta^{13}C$ values in Houzhai watershed. (d) The variation of $\delta^{13}C$ values in surface water and groundwater in Chenqi catchment.

Figure 5(a) The $\delta^{13}C$ values of soil collected at four different locations (A to D) on Tianlong Mountain. The $\delta^{13}C$ values of two transects of a ditch between two hills with four depths in Chenqi (b) CQ-1 and (c) CQ-2.

Figure 6 (a) The $\delta^{13}C$ values of arbor plants in Tianlong Mountain. (b) The $\delta^{13}C$ values of leaves, twig and roots of tree in Chenqi.

Figure 7 Season series analysis of mixing model results for Chenqi and Houzhai.

Figure 8 The Piper diagram of cationic and anion in surface water and groundwater in Chenqi and Houzhai watershed.

Figure 9 Component loadings of principal component analysis of Chenqi and Houzhai watershed

Figure 10 ^{13}C cycle in a nested karst watershed and proportion of carbon sources in the river.

Figure 1

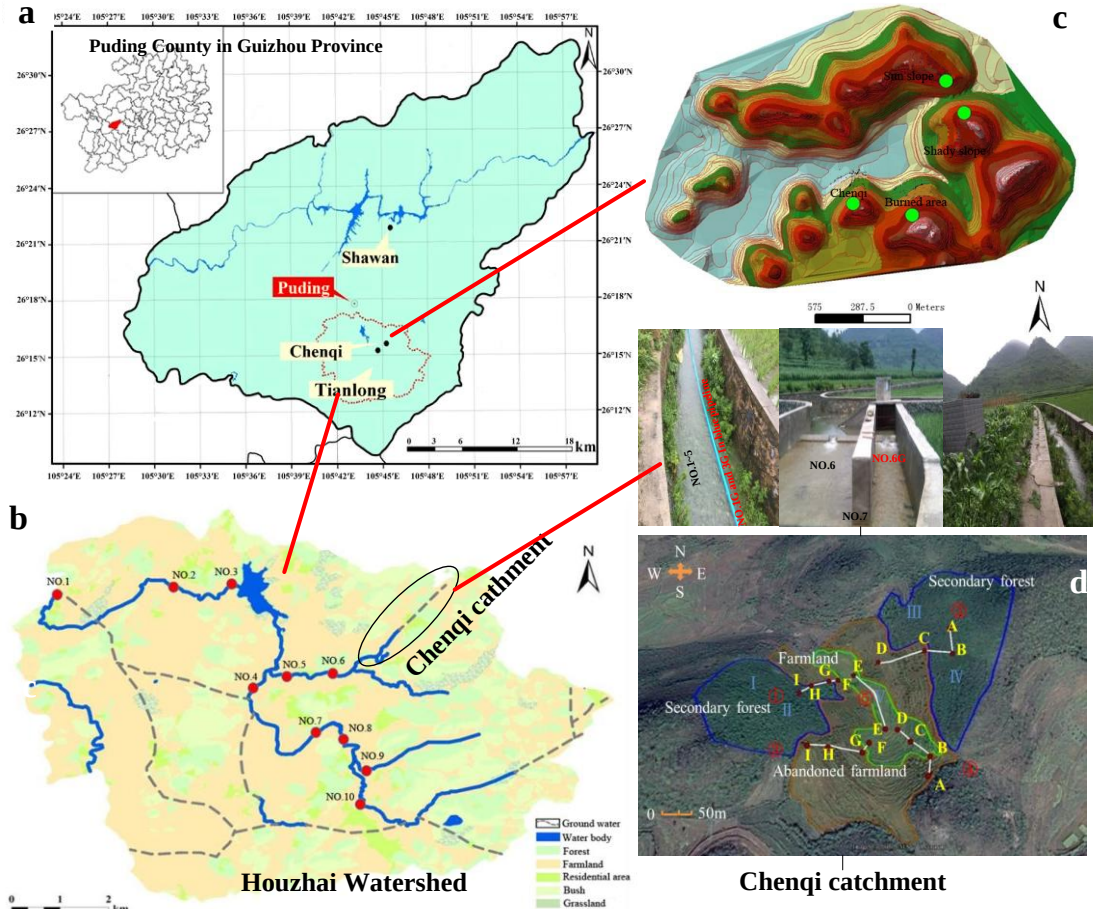

Figure 2

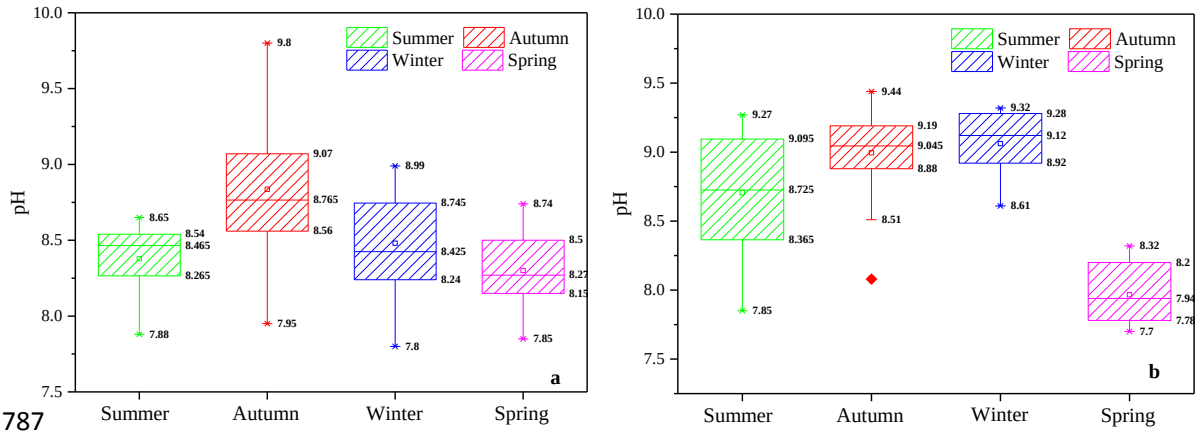
Summer
Autumn
Winter
Spring
pH
a
b
9.8
9.07
8.99
8.74
8.65
8.54
8.465
8.265
7.88
8.765
8.56
7.95
8.745
8.425
8.24
7.8
8.5
8.27
8.15
7.85
9.27
9.095
8.725
8.365
7.85
9.44
9.19
9.045
8.88
8.51
9.32
9.28
9.12
8.92
8.61
8.32
8.2
7.94
7.7

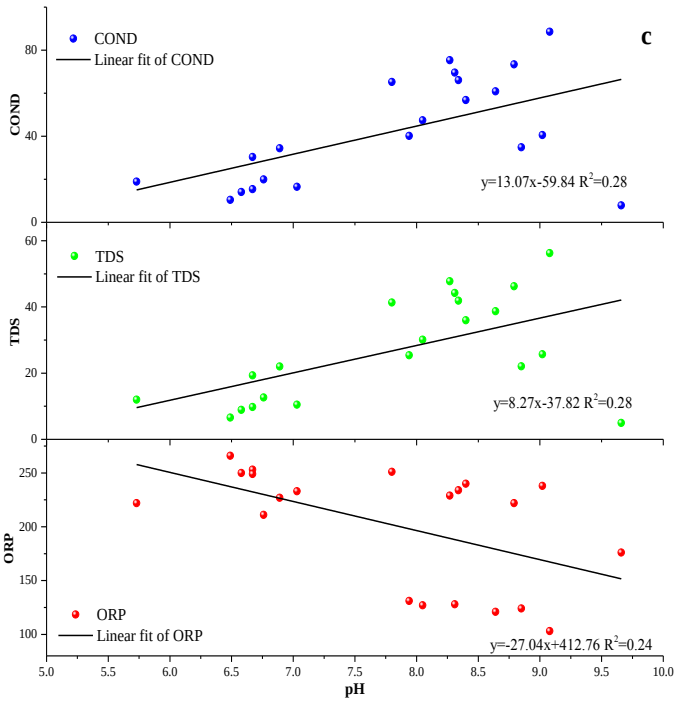
COND
Linear fit of COND
y=13.07x-59.84 R²=0.28
TDS
Linear fit of TDS
y=8.27x-37.82 R²=0.28
ORP
Linear fit of ORP
y=-27.04x+412.76 R²=0.24
pH
c

Figure 3

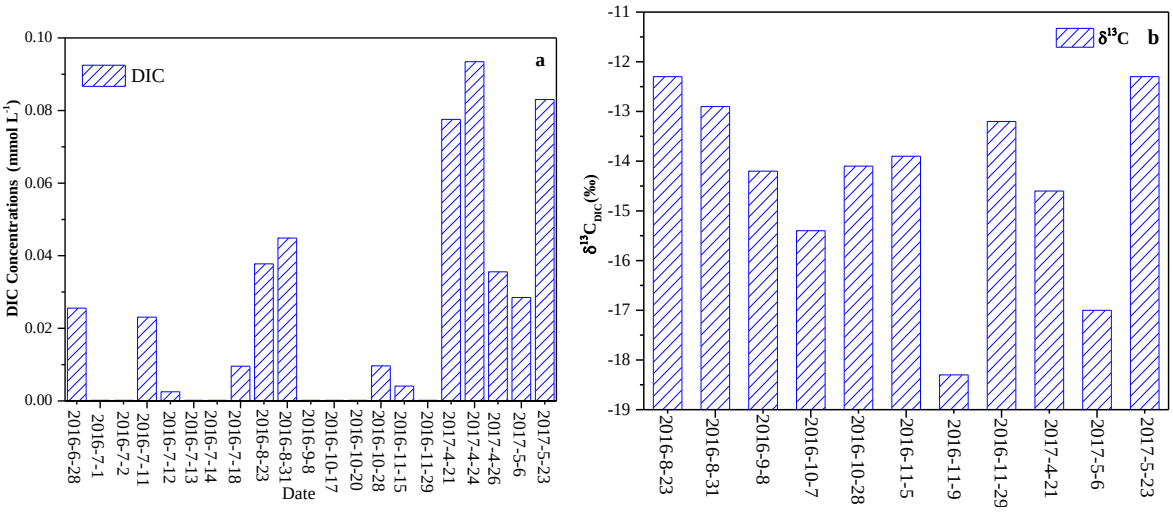
a
DIC
DIC Concentrations (mmol L-1)
0.10
0.08
0.06
0.04
0.02
0.00
2016-6-28
2016-7-1
2016-7-2
2016-7-11
2016-7-12
2016-7-13
2016-7-14
2016-7-18
2016-8-23
2016-8-31
2016-9-8
2016-10-17
2016-10-20
2016-10-28
2016-11-15
2016-11-29
2017-4-21
2017-4-24
2017-4-26
2017-5-6
2017-5-23
Date
b
δ13C
δ13CDIC (‰)
-11
-12
-13
-14
-15
-16
-17
-18
-19
2016-8-23
2016-8-31
2016-9-8
2016-10-7
2016-10-28
2016-11-5
2016-11-9
2016-11-29
2017-4-21
2017-5-6
2017-5-23

Figure 4

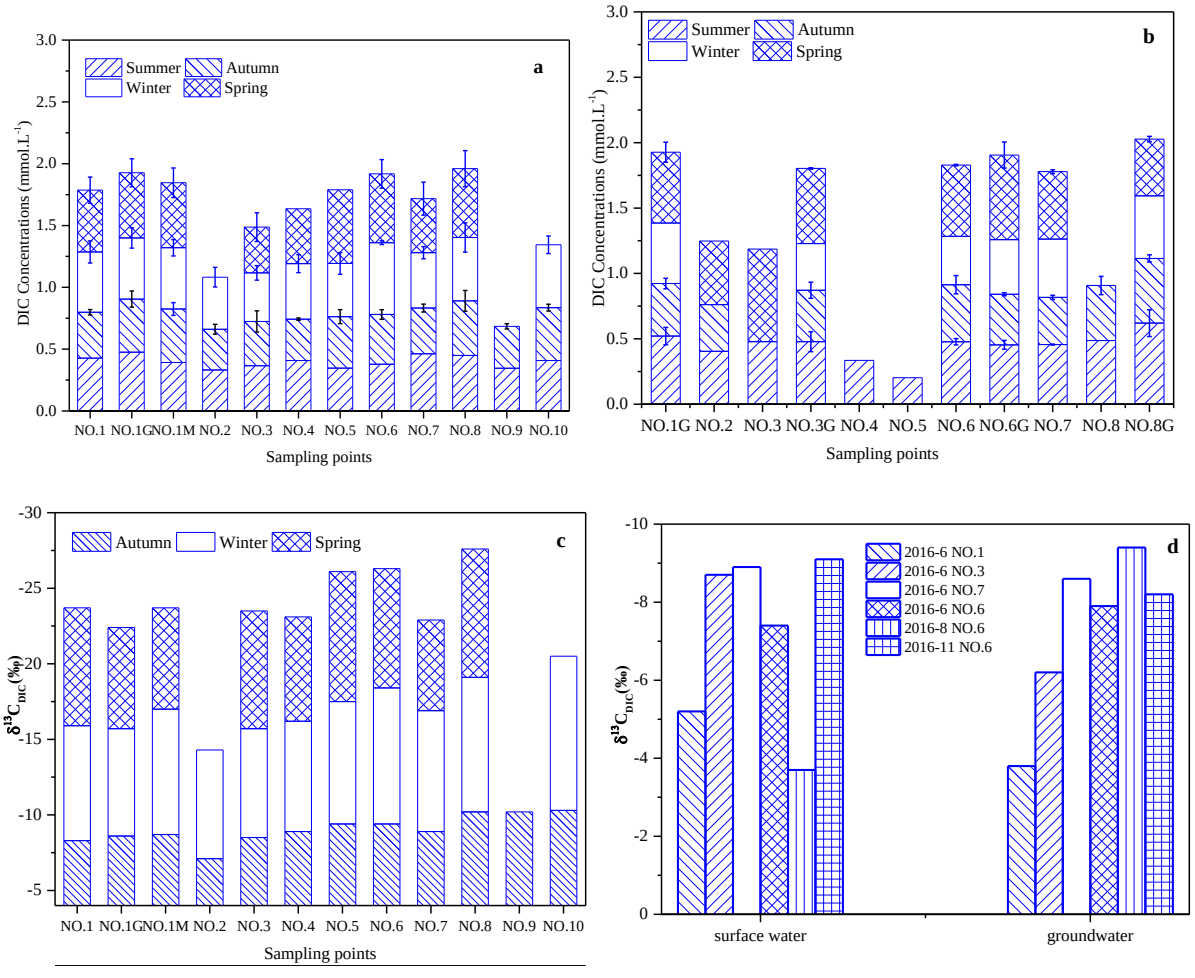
a
Summer
Autumn
Winter
Spring
DIC Concentrations (mmol.L-1)
NO.1 NO.1G NO.1M NO.2 NO.3 NO.4 NO.5 NO.6 NO.7 NO.8 NO.9 NO.10
Sampling points
b
NO.1G NO.2 NO.3 NO.3G NO.4 NO.5 NO.6 NO.6G NO.7 NO.8 NO.8G
c
δ13CDIC (‰)
d
2016-6 NO.1
2016-6 NO.3
2016-6 NO.7
2016-6 NO.6
2016-8 NO.6
2016-11 NO.6
surface water
groundwater

820

821

822

823

824 **Figure 5**

825

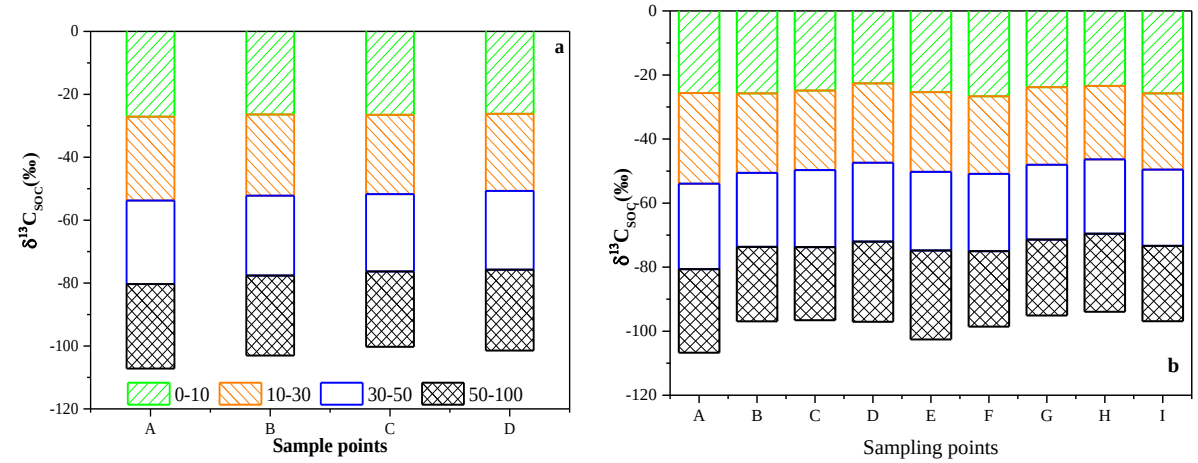

826

827

828

829

830

831

Figure 6

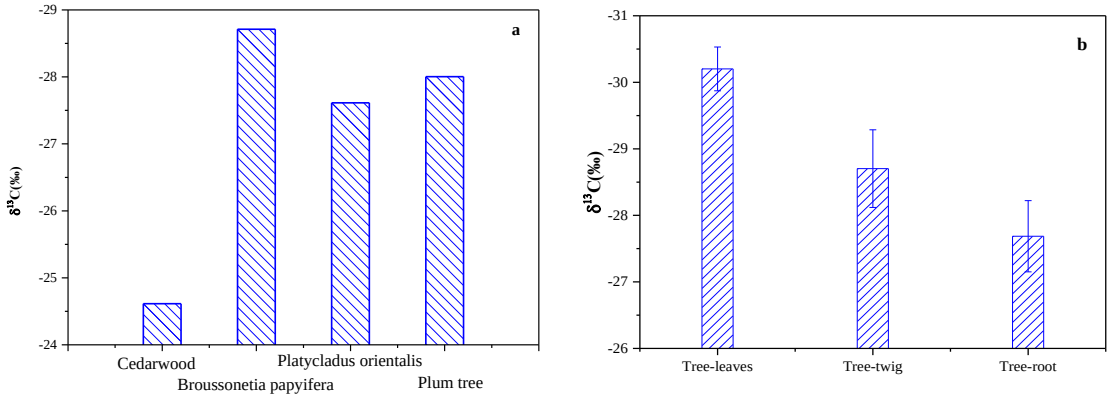
a
δ13C(‰)
-29
-28
-27
-26
-25
-24
Cedarwood
Broussonetia papyifera
Platycladus orientalis
Plum tree
b
δ13C(‰)
-31
-30
-29
-28
-27
-26
Tree-leaves
Tree-twig
Tree-root

Figure 7

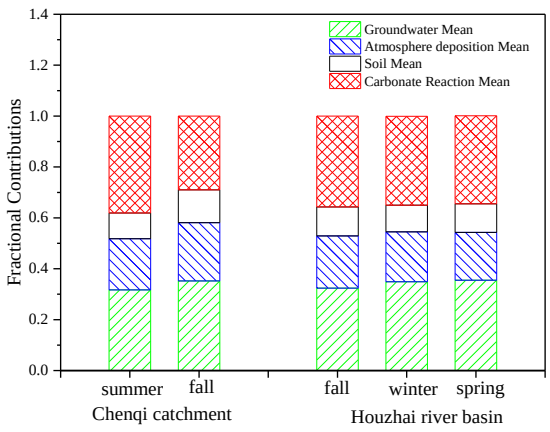
Groundwater Mean
Atmosphere deposition Mean
Soil Mean
Carbonate Reaction Mean
Fractional Contributions
1.4
1.2
1.0
0.8
0.6
0.4
0.2
0.0
summer
fall
fall
winter
spring
Chenqi catchment
Houzhai river basin

Figure 8

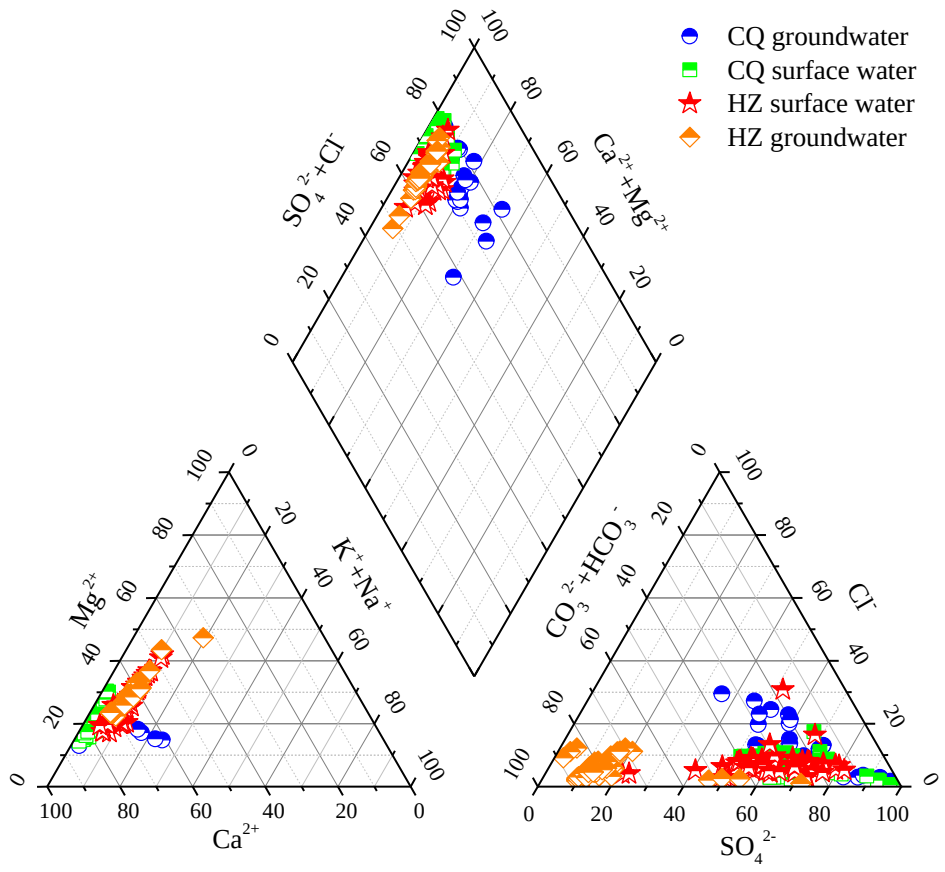
CQ groundwater
CQ surface water
HZ surface water
HZ groundwater
$SO_4^{2-}+Cl^-$
$Ca^{2+}+Mg^{2+}$
Mg^{2+}
K^++Na^+
Ca^{2+}
$CO_3^{2-}+HCO_3^-$
Cl^-
SO_4^{2-}

Figure 9

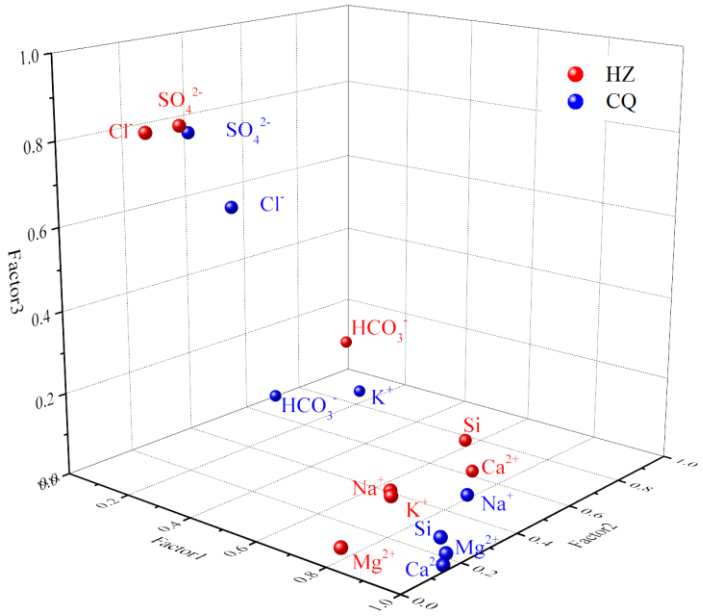
HZ
CQ
Factor3
Factor1
Factor2
1.0
0.8
0.6
0.4
0.2
0.0
SO_4^{2-}
Cl^-
HCO_3^-
K^+
Si
Ca^{2+}
Na^+
Mg^{2+}

Figure 10

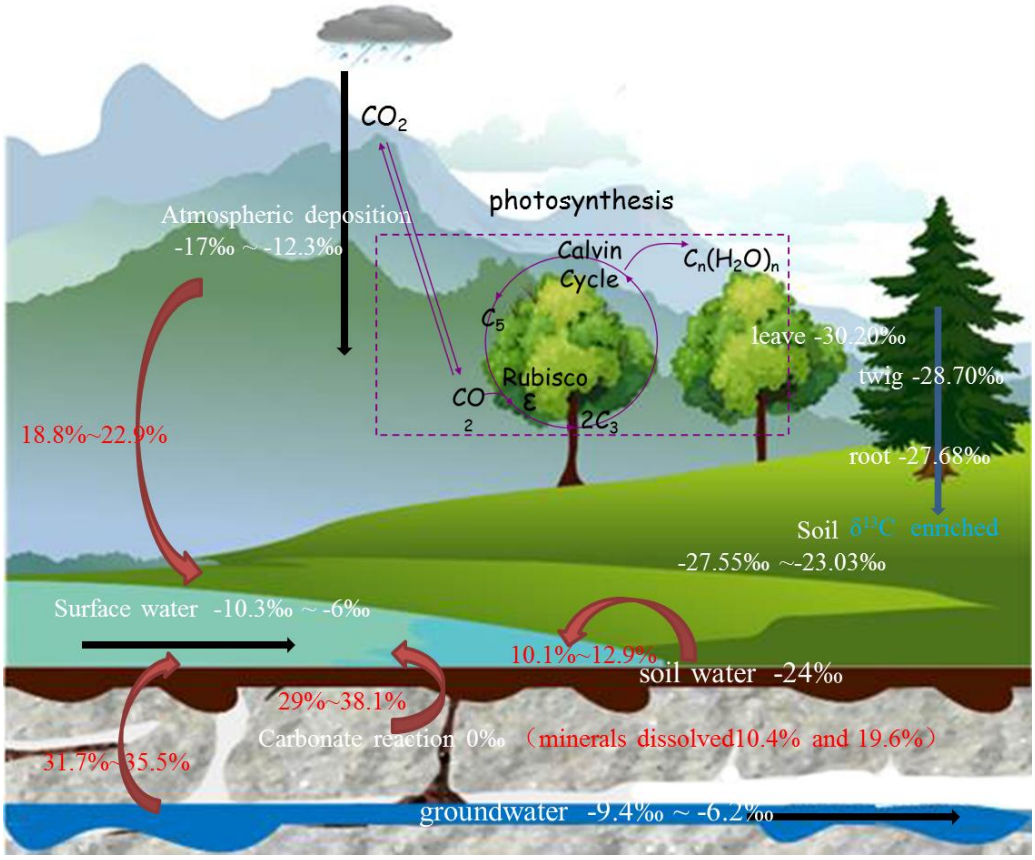
CO_2
photosynthesis
Atmospheric deposition
-17‰ ~ -12.3‰
Calvin Cycle
$C_n(H_2O)_n$
C_5
Rubisco
ε
CO_2
$2C_3$
leave -30.20‰
twig -28.70‰
root -27.68‰
18.8%~22.9%
Soil δ13C enriched
-27.55‰ ~-23.03‰
Surface water -10.3‰ ~ -6‰
10.1%~12.9%
soil water -24‰
29%~38.1%
Carbonate reaction 0‰ （minerals dissolved10.4% and 19.6%）
31.7%~35.5%
groundwater -9.4‰ ~ -6.2‰